# Magnetorheological Fluid for Levitation Migration Technology

Guang Yang* and ZhuPing Chen*

*Faculty of Mechanical Engineering, Jimei University, Xiamen 361021, China*

**Abstract:** The dispersed particles of magnetorheological fluid form stable chain-like clusters under the magnetic field, and show an effect of controllable flowability and shape. Based on this characteristic, using migration magnetic acted on the magnetorheological fluid, the object directional migration can be realized, and then the magnetorheological fluid forms levitation at the same time, which has like fluctuation behavior. The principle of magnetorheological fluid levitation migration, the levitation magnetic circuit design, the magnetic field strength and the magnetic force were separately discussed in this paper. In this study, the finite element method was used to numerically simulate the influence wedge-like of magnetic force applied on the magnetic particles in magnetorheological fluid. The relationships were given between flux and air gap width, magnetic field intensity and air gap width, flux and air gap angle, magnetic field intensity and air gap angle. The magnetic force applied on the magnetic particles in magnetorheological fluid has been calculated with virtual work method and Maxwell stress tensor method. The magnetorheological fluid levitation height was determined by using the MSL micrometer and aerosol migration feasibility was confirmed experimentally.

**Keywords:** Levitation migration, magnetic circuit, magnetorheological fluid (MRF), finite element analysis, magnetic force.

## 1. INTRODUCTION

MRF is a new type of function material. MRF is formed by combining a non-magnetorheological fluid with uniformly dispersed small particles, which have high permeability and low hysteresis. The behaviour of MRF reversibly changes from the linear viscous fluid to non-linear high viscoplasticsolid in milliseconds when a magnetic field is applied. MRF has been widely applied in various engineering fields. MRF has many potential applications in areas of mechanical engineering including seals, electric machines, vibration dampers, sensors, and lubrications [1-6].

Of particular concern is that this reasonable structure of magnetic field can form the different shape of MRF. Takimoto J *et al*. [7], studied shear stress and cluster structure of MRF levitations under tilted magnetic field, the results were shown the fluids are easier to flow in one direction than reverse direction and dispersed particles form stable chain-like clusters even under the tilted magnetic field condition. In order to rapidly manufacture high-precision aspherical mirrors made from RB-SiC, Cheng H.B. *et al.* [8], described a novel aspheric manufacturing system equipped with MRF technology, an electromagnet located directly under the polishing wheel uses specially designed pole pieces to induce a strong local magnetic field gradient across the top section of the wheel.

The finite element method was used to numerically simulate magnetic force acting on the magnetic particles in MRF under wedge-like magnetic field. The magnetic force acting on the magnetic particles in MRF was calculated with virtual work method and Maxwell stress tensor method.

*Address correspondence to these authors at the Faculty of Mechanical Engineering, Jimei University, Xiamen 361021, China; Tel: +86-13859921923; E-mails: yangg999@126.com, zooparkchen@126.com

This paper develops an effective structure of magnetic field for the MRF can be partially raised plastic solids. Using migration magnetic pole acted on the MRF, the object directional migration can be realized, and then the levitation of MRF was formed at the same time, which has like fluctuation behavior. Discussions were presented in this paper on the principle of MRF levitation migration, the levitation magnetic circuit design, the magnetic field strength and the magnetic force. The MRF levitation height was determined by using the MSL micrometer and aerosol migration feasibility was confirmed experimentally.

## 2. MIGRATION THEORY OF MRF LEVITATION

Migration theory of MRF levitation is shown in Fig. (**1**). Two pairs of magnetic poles placed in the horizontal plane, respectively, MR fluid, in the tray, placed on the top of the magnetic poles. The magnetic poles were made levitation of MRF and then the levitation has a height. MRF phase was transformed from liquid into solid, while strong shear stress was come into being. The left pole was moved to the right by certain velocity and wave was come into being on top of the MRF. This solid wave was can pushed object move. The object was moved to the levitation, which corresponding to right fixed magnetic pole, the object was stopped, to achieve the positioning of object. This move was can greatly reduced the friction of levitation and noise, and improved response time. This way was had many advantages, compared with the traditional mechanical transmission.

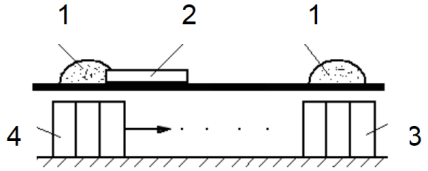


**Fig. (1).** Migration theory of MRF levitation. **1**. levatation of MRF, **2**. Object, **3**. Fixed magnetic poles, **4**. Migration magnetic poles.

1874-088X/11 2011 Bentham Open

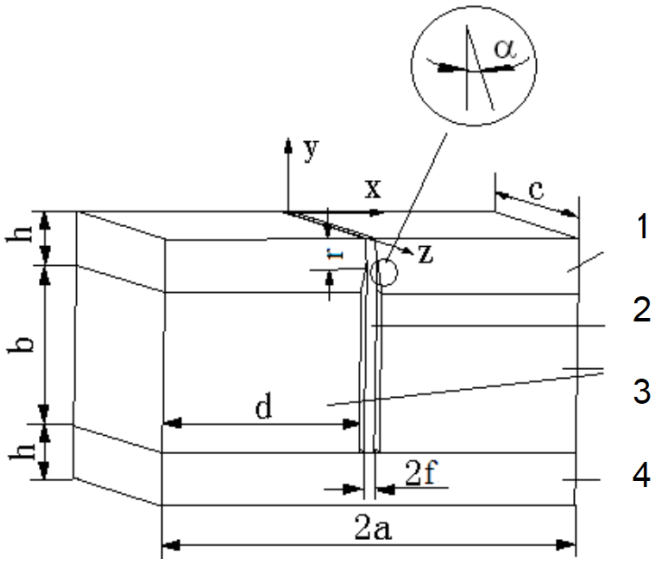


**Fig. (2).** Magnetic circuit structure. **1**. Upper magnetic yoke, **2**. Aluminium plate, **3**. Permanent magnets, **4**. Nether magnetic yoke.

### 2.1. Magnetic Circuit Structure

The design of magnetic circuit structure was become very important, in order to the MRF was formed wave and the wave was can pushed object move. Magnetic circuit structure of levitation of MRF was used as shown in Fig. (**2**). The two upper magnetic yokes were above the poles. The poles and upper magnetic yokes were separated by an insulator. Nether magnetic pole yoke was placed on the two poles below, as a whole. U-shaped magnetic loop and wedge-shaped magnetic head were formed a high gradient magnetic field in the vertical direction of interspace of two upper magnetic yokes.

### 2.2. Magnetic Leakage Coefficient

Two above magnetic yoke were separated by aluminum slice. The aluminum is not magnetic conductor and air gap was formed between the two magnetic yoke, which thickness was equivalent the size of aluminum. In this magnetic circuit structure, magnetic leakage coefficient was given as follows:

$$K_f = 1 + \frac{2f}{S_g}[1.7l_1 \cdot (\frac{a-f}{a+f}) + 1.4h + 0.94b\sqrt{\frac{l_2}{2a} + 0.25}]. \quad (1)$$

where $l_1$ is the unilateral vertical cross-section perimeter of magnetic pole, $l_1 = 2(h+c)$ ; $l_2$ is the level of unilateral cross-section perimeter of magnetic pole, $l_2 = 2(d+c)$ ; $S_g$ is the air-gap area, $S_g = c \cdot r$.

### 2.3. Scalar Magnetic Potential

Magnetic field strength in a point is equal to negative gradient of this point's scalar magnetic potential. First, the equations of scalar magnetic potential were derived in the magnetic field, and then spatial distribution of magnetic field strength was derived. Permanent magnet provides a constant magnetic field. The above midpoint magnetic field of the magnetic poles was inspected and two-dimensional analysis to it was provided. In the interval $y \geq 0, -a \leq x \leq a$, the simplified two-dimensional Laplace equation is:

$$\frac{\partial^2 u}{\partial x^2} + \frac{\partial^2 u}{\partial y^2} = 0. \quad (2)$$

General solution of equation (2) was derived using separation of variables, and into exponential form:

$$u(x,y) = \sum_{n=1}^{\infty}(K_{1n}\cos\beta x + K_{2n}\sin\beta x)(K_{3n}e^{\beta y} + K_{4n}e^{-\beta y}). \quad (3)$$

where $K_{1n}, K_{2n}, K_{3n}, K_{4n}, \beta$ are undetermined coefficients. The boundary conditions of magnetic field are as follows:

1. Infinity is the zero magnetic potential, that is, $y = \infty, u = 0$.
2. $y$ axis is equipotent line to the infinite distance, that is, $x = 0, u = 0$.
3. In points $x = \pm a$, magnetic field lines parallel to the $y$ axis and point to infinity, that is, $x = \pm a, \frac{\partial u}{\partial x} = 0$.
4. In the $x$ axis, in the interspace, magnetic field is approximate uniform distribution:

$y = 0, -a \leq x \leq a$, $u = \frac{B_g}{\mu_0}x$. Where, $B_g$ is flux density of interspace, $B_g = \frac{B_m \cdot S_m}{K_f \cdot S_g}$, $B_m$ is the magnetic induction intensity of permanent magnet working gap, $S_m$ is working area, $S_m = c \cdot d$; $\mu_0$ is the vacuum magnetic permeability.

5. For the upper and nether magnetic yoke, each magnetic bit is a constant. From the continuity, in point $y = 0$, we have

$$u = \begin{cases} \frac{B_g}{\mu_0}f, f \leq x \leq a \\ -\frac{B_g}{\mu_0}f, -a \leq x \leq -f \end{cases}. \quad (4)$$

Using the boundary conditions 1, 2 and equation (3), we have $K_{1n} = 0$, $K_{3n} = 0$, and equation (3) becomes

$$u(x,y) = \sum_{n=1}^{\infty} K_n \sin(\beta x)e^{-\beta y}. \quad (5)$$

Then the boundary conditions were introduced into the equation (5), the expression of $\beta$ is

$$\beta = \frac{2n-1}{2a}\pi \quad n = 1,2,3\ldots \quad (6)$$

In value $y = 0$, the magnetic potential equation is obtained by the boundary conditions 4 and 5:

$$u=\begin{cases}\dfrac{B_g}{\mu_0}f, f\le x\le a\\ \dfrac{B_g}{\mu_0}x, -f\le x\le f\\ -\dfrac{B_g}{\mu_0}f, -a\le x\le -f\end{cases}. \quad (7)$$

$$u(x,0)=\sum_{n=1}^{\infty}K_n\sin(\frac{2n-1}{2a}\pi x). \quad (8)$$

$K_n$ is solved using sine function's orthogonality. The equation (8) was multiplied by expression $\sin[(2m-1)\pi x/2a]$, and integrated in the scope $[-2a,2a]$, we have

$$\begin{aligned}&\int_{-2a}^{2a}u(x,0)\sin(\frac{2m-1}{2a}\cdot\pi\cdot x)dx\\ &=2[\int_0^f\frac{B_g\cdot x}{\mu_0}\sin(\frac{2m-1}{2a}\cdot\pi\cdot x)dx\\ &+\int_f^a\frac{B_g\cdot x}{\mu_0}\sin(\frac{2m-1}{2a}\cdot\pi\cdot x)dx]\\ &=\frac{8a^2B_g\sin(\frac{2m-1}{2a}\cdot\pi\cdot f)}{\pi^2(2m-1)^2\mu_0}\end{aligned}. \quad (9)$$

Right side function of equation (8) is integrated, we have

$$\begin{aligned}&\int_{-2a}^{2a}\sum_{n=1}^{\infty}K_n\sin(\frac{2n-1}{2a}\cdot\pi\cdot x)\cdot\sin(\frac{2m-1}{2a}\cdot\pi\cdot x)dx\\ &=\sum_{n=1}^{\infty}K_n\int_{-2a}^{2a}\sin(\frac{2n-1}{2a}\cdot\pi\cdot x)dx\cdot\sin(\frac{2m-1}{2a}\cdot\pi\cdot x)dx\\ &=\begin{cases}0 & m\ne n\\ 2K_n\cdot a & m=n=0\end{cases}\end{aligned}. \quad (10)$$

Therefore, the coefficient $K_n$ is

$$K_n=\frac{4a\cdot B_g\cdot\sin(\frac{2n-1}{2a}\cdot\pi\cdot f)}{\pi^2(2n-1)^2\mu_0}. \quad (11)$$

and particular solution of scalar magnetic potential is as follows:

$$\begin{aligned}u(x,y)=&\sum_{n=1}^{\infty}\frac{4a\cdot B_g}{(2n-1)^2\mu_0}\sin(\frac{2n-1}{2a}\cdot\pi\cdot f)\\ &\cdot\sin(\frac{2n-1}{2a}\cdot\pi\cdot x)e^{-\frac{2n-1}{2a}\pi y}\end{aligned}. \quad (12)$$

### 2.4. Calculation of Magnetic Field Strength

Magnetic field strength is equal to negative scalar magnetic gradient, for the above mentioned magnetic field, we have

$$\vec{H}=-(\frac{\partial u}{\partial x}\vec{i}+\frac{\partial u}{\partial y}\vec{j}). \quad (13)$$

The partial differential of particular solution of scalar magnetic potential is computed by equation (13), and we have

$$\vec{H}=\sum_{n=1}^{\infty}-A_n\cos(\beta\cdot x)e^{-\beta y}\vec{i}+\sum_{n=1}^{\infty}A_n\sin(\beta\cdot x)e^{-\beta y}\vec{j}. \quad (14)$$

where

$$A_n=K_n\cdot\beta=\frac{2B_g\cdot\sin(\beta\cdot f)}{\pi(2n-1)\cdot\mu_0}. \quad (15)$$

The required magnetic field strength is obtained, which can made levitation of MFR. Withstanding magnetic force of magnetic particles is calculated. Remaining magnetic induction intensity of spherical particles in magnetic field is

$$\vec{B}=\frac{3\mu\mu_0}{\mu+2\mu_0}\cdot\vec{H}. \quad (16)$$

where $\mu$ is magnetic permeability of magnetic particle; $\vec{H}$ is the magnetic field strength in position of magnetic particle. Magnetic particles are very small, therefore, in the magnetic filed, each particle is regarded as a magnetic dipole and its magnetic dipole moment is

$$\vec{m}=\Delta V\cdot\vec{M}=\Delta V\cdot X_m\cdot\frac{\vec{B}}{\mu}. \quad (17)$$

where $\Delta V$ is the volume of magnetic particle; $X_m$ is the magnetic susceptibility of magnetic particle; $\vec{M}$ is magnetization strength of magnetic particle.

In magnetic field, withstanding magnetic force of magnetic particles is

$$\vec{F}_m=(\vec{m}\cdot\nabla)\vec{B}. \quad (18)$$

From equation (16), (17) and (18), we have

$$\vec{F}_m=\Delta V\cdot X_m\frac{3\mu_0^2}{\mu+2\mu_0}(\vec{H}\cdot\nabla)\vec{H}. \quad (19)$$

where

$$(\vec{H}\cdot\nabla)\vec{H}=\sum_{n=1}^{\infty}-A_n\cos(\beta\cdot x)e^{-\beta y}\frac{\partial\vec{H}}{\partial x}+\sum_{n=1}^{\infty}A_n\sin(\beta\cdot x)e^{-\beta y}\frac{\partial\vec{H}}{\partial y}. \quad (20)$$

$$\frac{\partial\vec{H}}{\partial x}=\sum_{n=1}^{\infty}A_n\beta\sin(\beta\cdot x)e^{-\beta y}\vec{i}+\sum_{n=1}^{\infty}A_n\beta\cos(\beta\cdot x)e^{-\beta y}\vec{j}. \quad (21)$$

$$\frac{\partial\vec{H}}{\partial y}=\sum_{n=1}^{\infty}A_n\beta\cos(\beta\cdot x)e^{-\beta y}\vec{i}+\sum_{n=1}^{\infty}A_n\beta\sin(\beta\cdot x)e^{-\beta y}\vec{j}. \quad (22)$$

Therefore, the expression of magnetic force is

$$\vec{F}_m=F_x\vec{i}+F_y\vec{j}. \quad (23)$$

where

$$\begin{aligned}F_x=&\Delta V\cdot X_m\frac{3\mu_0^2}{\mu+2\mu_0}(\sum_{n=1}^{\infty}A_n\sin(\beta\cdot x)e^{-\beta y}\cdot\sum_{n=1}^{\infty}A_n\beta\cos(\beta\cdot x)e^{-\beta y}\\ &-\sum_{n=1}^{\infty}A_n\cos(\beta\cdot x)e^{-\beta y}\cdot\sum_{n=1}^{\infty}A_n\beta\sin(\beta\cdot x)e^{-\beta y})\end{aligned}. \quad (24)$$

$$F_y = -\Delta V \cdot X_m \frac{3\mu_0^2}{\mu + 2\mu_0} (\sum_{n=1}^{\infty} A_n \sin(\beta \cdot x) e^{-\beta y} \cdot \sum_{n=1}^{\infty} A_n \beta \cos(\beta \cdot x) e^{-\beta y} + \sum_{n=1}^{\infty} A_n \cos(\beta \cdot x) e^{-\beta y} \cdot \sum_{n=1}^{\infty} A_n \beta \sin(\beta \cdot x) e^{-\beta y}) \quad (25)$$

The levitation height of MRF increases as the magnetic force increase. In order to move object with certain thickness, levitation height of MRF at least is higher than the object thickness. From the previous expressions we can see that the volume of magnetic particles and the magnetic susceptibility are proportionable to the magnetic field strength. In addition, the magnetic permeability of magnetic particles, the magnetic induction intensity of permanent magnet working gap, work area, magnetic leakage coefficient and area of air gap were affected the magnetic force.

From equation (25) shows that the magnetic force acting on the magnetic particles in MRF was expanded by total of infinite items and calculated by limited items, but the error will change with the reservation number of limited items, and then the finite element method was used to numerically simulate the influence wedge-like of magnetic force applied on the magnetic particles in MRF.

## 3. FINITE ELEMENTANALYSIS OF MAGNETIC FIELD

### 3.1. Material Properties and Modeling

The finite element analysis of magnetic field was calculated by electromagnetic field module of ANSYS program. The permanent magnet is N40H, coercive force is 900kA/m, remanence is 1.28T and the demagnetization curve is reduced to as a straight line. Materials of magnetic yoke were used electric iron yoke, and the relative permeability is 1800. The experimental MRF materials were used water-based material, with spherical carbonyl iron as the magnetic particles. The MRF initial viscosity is 0.5Pas, radius of magnetic particles is $2.5\times10^{-6}$m and relative permeability is 2000. Relative permeability of air is 1. Values given above were assumed at 20°C.

As the air gap length is much greater than its width, so the finite element analysis is reduced to two-dimensional electromagnetic field analysis. The points, lines, planes geometry creation of the permanent magnet and the magnetic yoke were completed using bottom-up modeling method. In order to calculate the magnetic force, air model was created, which was between magnetic particles and the upper magnetic yoke. The scalar magnetic potential to satisfy the standards of the Laplace equation, and its parallel boundary conditions are automatically satisfied in the program, in the magnetic field of the plane stability in Cartesian coordinate system.

### 3.2. Mesh

Parameters of the calculations are as follows: $a$=50mm, $b$=60mm, $c$=70mm, $d$=45mm, $r$=10mm, $f$=4mm, $h$=15mm. Therefore, the magnetic leakage coefficient is $K_f = 5.08$ by calculation. PLANE53 is 4 polygon and 8 node element, witch is based on magnetic vector potential equation and is applicable to low frequency electromagnetic field analysis. PLANE53 element was used in this two-dimensional electromagnetic field analysis. The magnetic field structure was modeled as 2272 PLANE53 elements and 7172 nodes. The finite element model of wedge-shaped magnetic field is shown in Fig (**3**). The meshes at air gap were subdivided in order to get accurate results of magnetic field strength.

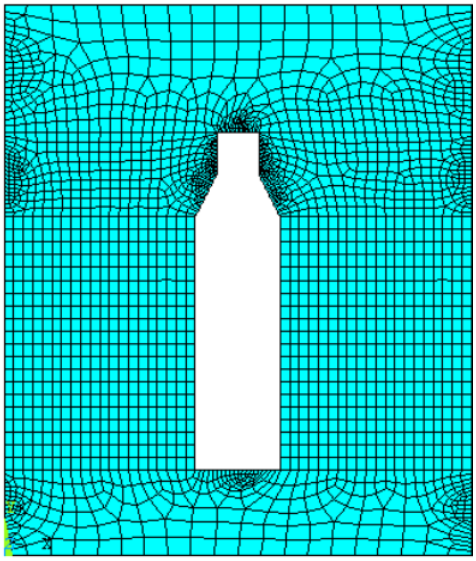

**Fig. (3).** Finite element model.

### 3.3. Results and Discussion

#### *3.3.1. Magnetic Flux and Magnetic Field Strength*

The magnetic field is simply connected iron area and the DSP method was selected to calculate. The Frontal solver was used for two-dimensional analysis of static magnetic field. The magnetic flux density vector distribution and magnetic field intensity vector distribution are shown in Figs. (**4**, **5**). As can be seen from Figs. (**4**, **5**), the magnetic flux density of upper air gap is denser, magnetic field intensity is stronger, and here MRF levitation can created.

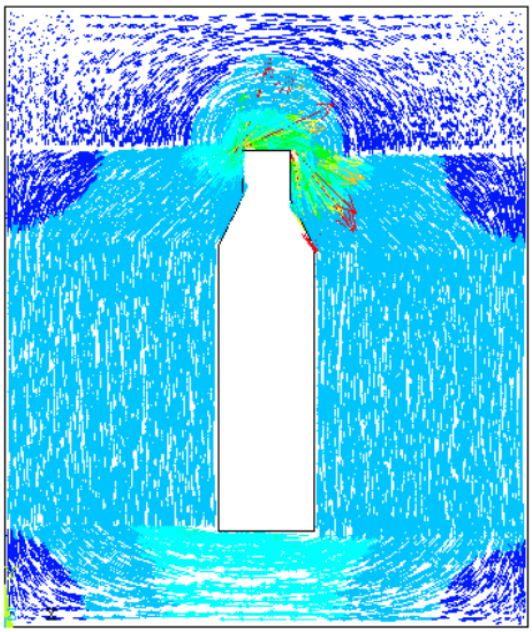

**Fig. (4).** Magnetic flux density vector.

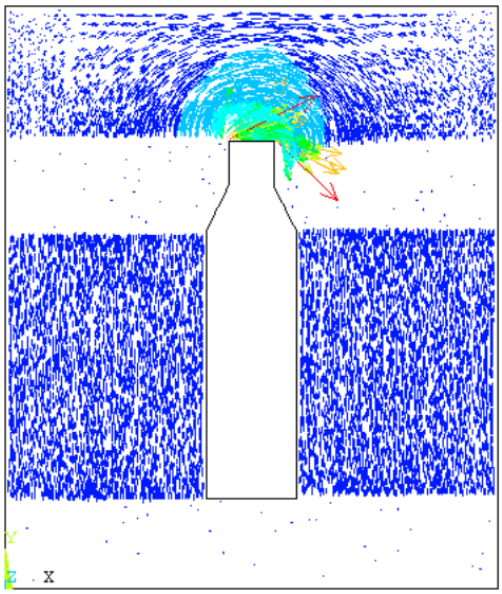

**Fig. (5).** Magnetic field intensity vector.

In order to optimize the magnetic field, the relationships were given between flux and air gap width, magnetic field intensity and air gap width, flux and air gap angle, magnetic field intensity and air gap angle. As can be seen from Figs. (**4**, **5**), the flux and magnetic field intensity can be changed with air gap size. The flux and magnetic field intensity increases as the air gap width decreases. The flux and magnetic field intensity increases as the air gap angle increases. However when the angle reached at 0.61rad, they began to decrease. The reason is that the larger magnetic field gradient increases as the air gap angle increases, but then the volume size of the permanent magnet becomes smaller, and magnetic field strength reduces.

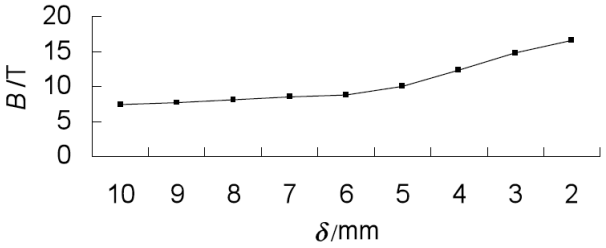


**Fig. (6).** Magnetic flux density in MRF working gap.

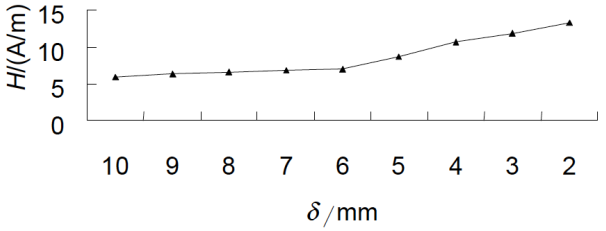


**Fig. (7).** Magnetic field strength in MRF working gap.

### *3.3.2. Analysis of the Magnetic Force*

In this section, the magnetic force applied on the magnetic particles in MRF has been calculated with virtual work method and Maxwell stress tensor method. Maxwell stress tensor method and the virtual work method are two methods for calculate electromagnetic force. The Maxwell stress tensor method is calculated by surface stress tensor matrix method, and virtual work method is calculated by the energy of the whole system.

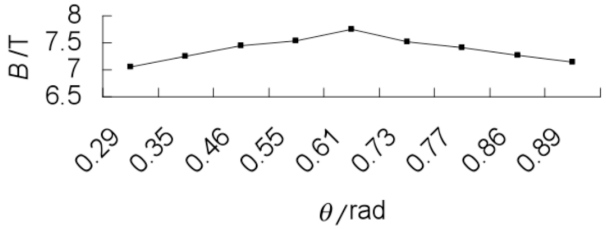


**Fig. (8).** Magnetic flux density for MRF working gap.

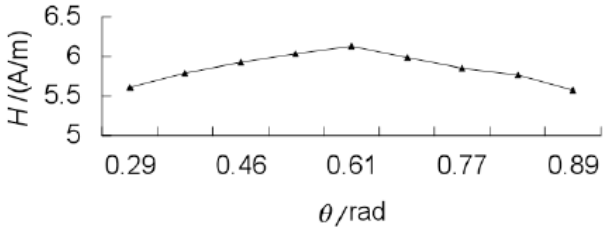


**Fig. (9).** Magnetic field strength for MRF working gap.

Curves of magnetic force for MRF working gap are shown in Figs. (**10**, **11**). Study results show that the magnetic force can be changed with change of air gap size. Magnetic force increases as the air gap width decreases. The magnetic force was $1.52\times10^{-8}$N, which was calculated by virtual work method as the air gap width was 10mm. The magnetic force was $4.02\times10^{-8}$N and increase 164%, which was calculated by virtual work method as the air gap width is 2mm. The magnetic force increases as the air gap angle increases. However, when the angle reached at 0.61rad, magnetic force began to decrease. The reason is that the larger magnetic field gradient increases as the air gap angle increases, but then the volume size of the permanent magnet becomes smaller, and magnetic field strength reduces. In addition, from Figs. (**10**, **11**) can be seen that the results obtained by Maxwell stress tensor method are generally higher than the results obtained by virtual work method.

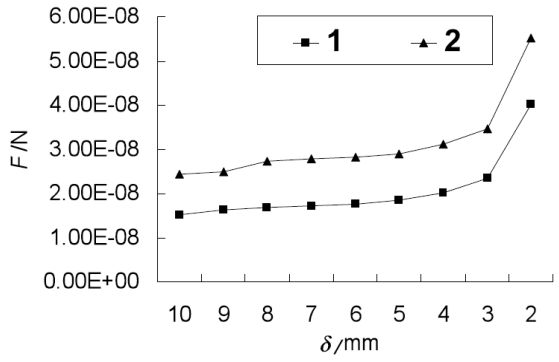


**Fig. (10).** Curves of magnetic force for MRF working gap. **1**. Virtual work method, **2**. Maxwell stress tensor method.

## 4. EXPERMRNTAL VERIFICATION

In order to validate the above theory is correct, the MRF levitation height and the levitation force were experimented using MSL micrometer and counter poise. Levitation migration was needed that the good flowability of MRF is good and has initial low viscosity and good rheological properties. The experimental MRF materials were used water-based material, with spherical carbonyl iron as the

magnetic particles. The MRF initial viscosity is 0.5Pas, radius of magnetic particles is $2.5\times10^{-6}$m and relative permeability is 2000. Yield stress is 20kPa, when magnetic field strength is 320kA/m.

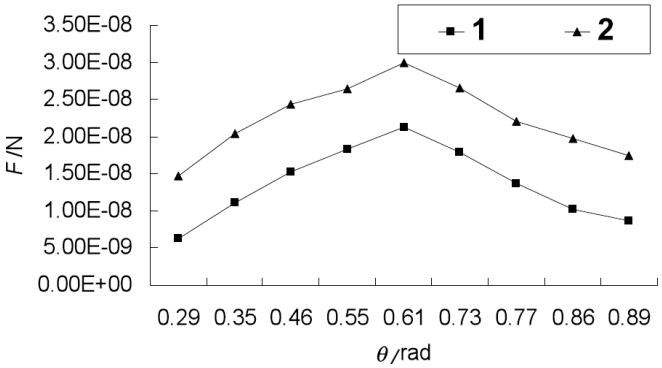


**Fig. (11).** Curves of magnetic force for MRF working gap. **1**. Virtual work method, **2**. Maxwell stress tensor method.

In the experiment, two poles at the same time were acted on the MRF and the tray was holded up by two ribbons. Schematic diagram of experimental verification is shown in Fig. (**12**). The whole device was placed on anti-vibration table, in order to avoid the interference of external low-frequency vibration. In order to reduce the error, micrometer probe always contacts with the center of counter poise. The micrometer readings were read with magnetic field and the levitation height was obtained.

Weight of the counter poise is equal to the double value of load. The test relationship between MRF levitation height and load is shown in Fig. (**13**). As can be seen from Fig. (**13**), the MRF levitation effect was good, in certain load scope. Levitation height gradually decreased as the load increases until both achieve dynamic equilibration.

Velocity $V=0.1$m/s was imposed on the left magnetic poles, the moving speed is 0.096m/s of counter poise tray by speed sensor. The tray was soon stopped, when it touched the ribbon, which corresponding to right fixed magnetic poles.

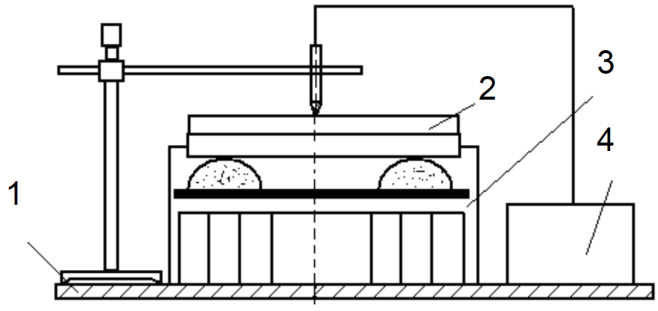


**Fig. (12).** Experimental equipment. **1**. Worktable, **2**. Object, **3**. Levitation equipment, **4**. MSL.

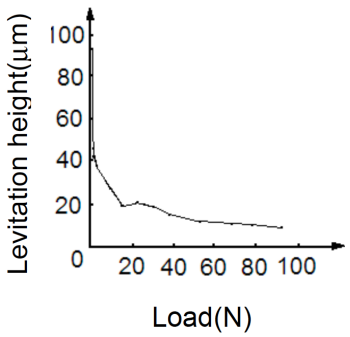


**Fig. (13).** Relationship between MRF levitation height and load.

## 5. CONCLUSIONS

A new technique for forming the levitation migration of MRF was presented. The present technique is based on the migration of wedge-like magnetic field. The finite element analysis was given, which is about magnetic force acting on the magnetic particles under wedge-like magnetic field. The relationships between flux, magnetic field intensity and magnetic force with air gap width and air gap angle were also discussed. The MRF levitation height and the levitation force were experimented using MSL micrometer and counter poise. The results obtained in this paper indicate that the present procedure is valid and effective.

## ACKNOWLEDGEMENTS

Project supported by the Science Foundation of Fujian Province (No:2010J01007) and Foundation of Jimei University Pan Jin-long(No:ZC2010018), China.

## REFERENCES

[1] Bica D, Vecas L, Rasa L. Preparation and magnetic properties of concentrated magnetic fluids on alcohol and water carrier liquids. Magn Magn Mater 2002; 252: 10-2.

[2] Vekas L, Potencz I, Bica D. The Behavior of Magnetic Fluids under Strong Nonuniform Magnetic Field in Rotating Seal. Magn Magn Mater 1987; 65: 223-6.

[3] Evsing SI, Sokolov NA. Development of magnetic fluid reciprocating motion seals. Magn Magn Mater 1990; 85: 253-6.

[4] Anton I, Desata I, Vekas L. Magnetic fluid seals some design problems and application. Magn Magn Mater 1987; 65: 379 -81.

[5] Choi SB, Lee SK. A hydro-mechanical model for hysteretic damping force prediction of ER damper: experimental verification. Sound Vibration 2001; 245:375-83.

[6] Coulomb JL, Meunier G. Finite element lmplementantion of virtual work principle for magnetic of electric force and torque computation. IEEE Trans Magn 1984; 2: 1894-6.

[7] Takimoto J, Takeda H, Masubuchi Y, Koyama K. Stress rectification in MR fluid under tilted magnetic field International. Modern Phys B 1999;13:2028-35.

[8] Cheng HB, Feng ZJ, Wang YW. Magnetorheological Finishing of Sic Aspheric Mirrors. Mater Manuf Processes 2005; 20:917-31.

Received: August 26, 2010 Revised: November 26, 2010 Accepted: December 22, 2010